Available online at www.sciencedirect.com
SCIENCE DIRECT
International Journal of Heat and Fluid Flow 27 (2006) 220–228
International Journal of HEAT AND FLUID FLOW
www.elsevier.com/locate/ijhff

Numerical and experimental predictions of heterogeneous condensate flow of moist air in cooled pipe

Kei Sakakura [a,*], Satoru Yamamoto [b]

[a] Process Development Center, Idemitsu Kosan Co., Ltd, 1-1 Anesaki-Kaigan, Ichihara, Chiba 299-0193, Japan
[b] Department of Computer and Mathematical Sciences, Tohoku University, Sendai 980-8579, Japan

Received 21 October 2004; received in revised form 14 July 2005; accepted 9 August 2005
Available online 9 November 2005

Abstract

Condensate flows of moist air in a cooled pipe are numerically investigated by using the preconditioning method for solving incompressible and compressible Navier–Stokes equations with additional equations and source terms for condensate flows. The corresponding experiments are also conducted with the calculated results being compared with the experimental results. The present numerical method can apply not only to compresssible flows, but also to flows at a very low Mach number with condensation without the stiffness of solution. Very slow flows of moist air in a cooled pipe (in which the wall is partially cooled) are calculated using this method by assuming heterogeneous condensation. Then, humidity loss due to condensation when stream of moist air flow in the cooled pipe is numerically and experimentally predicted.

Keywords: Condensate flow; Moist air; Heterogeneous nucleation; Cooled pipe

1. Introduction

The earth's atmosphere includes a finite amount of water vapor. Moist air occasionally condenses in wind tunnel experiments. The onset of condensation may be dominated by homogeneous nucleation. Homogeneous nucleation occurs suddenly from pure water vapor without a nucleus in a high-supersaturated condition. The atmosphere also includes small particulates, such as soot and aerosols. These small particulates may behave as a nucleus of condensation when the water vapor in moist air saturates. The moist air largely depends on weather conditions. Then, the phase change of water from vapor to liquid is mainly dominated by heterogeneous nucleation, which occurs in a saturated condition.

Condensation phenomena are observed not only in meteorological problems, but also in current engineering problems such as those posed by steam turbines, power plants, fuel cells, and chemical vapor deposits (CVD). The condensed matter may adversely affect efficiency or performance. Condensation may also cause erosion in a pipe due to wet steam or a stream of moist air with chemistry such as the oxides of nitrogen and sulfur. Therefore, the mechanism of condensation that adversely affects performance and safety should be resolved. Although many experimental and numerical studies have been conducted on nonequilibrium condensate flows associated with homogeneous nucleation in past decades (Hill, 1966; Moses and Stein, 1978; Schnerr, 1989; Young, 1992), the mechanism of condensate flows with heterogeneous nucleation has yet to be sufficiently resolved. The difficulty in understanding heterogeneous condensation is mainly due to the difficulty in measuring such quantitative values as condensate mass fraction and the number density of particulates in the flows.

Recently, Yamamoto et al. (2000) developed a numerical method for solving transonic viscous flows around the ONERA M6 wing by assuming atmospheric wind tunnel

* Corresponding author. Tel./fax: +81 22 217 6988.
E-mail addresses: kei.sakakura@si.idemitsu.co.jp (K. Sakakura), yamamoto@caero.mech.tohoku.ac.jp (S. Yamamoto).

0142-727X/$ - see front matter © 2005 Elsevier Inc. All rights reserved.
doi:10.1016/j.ijheatfluidflow.2005.08.006

Nomenclature

C_p	specific heat at constant pressure	x_i	Cartesian coordinates ($i = 1,2$)
e	total internal energy per unit volume	β	condensate mass fraction
H	total enthalpy	Γ	preconditioning matrix
I_c	nucleation rate	Γ_c	condensate mass generation rate
J	Jacobian of transformation	ξ_i	general curvilinear coordinates ($i = 1,2$)
n	number density of nucleus	ρ	total density
p	static pressure	ρ_v	density of water vapor
Re	Reynolds number	μ	molecular viscosity
T	static temperature	δ_{ij}	Kronecker's delta
U_i	contravariant velocities ($i = 1,2$)	τ_{ij}	viscous stress tensors ($i,j = 1,2$)
u_i	physical velocities ($i = 1,2$)	κ	heat conductivity
t	physical time		

conditions. Nonequilibrium condensation dominated by homogeneous nucleation is taken into account in the calculations. Yamamoto (2003) also developed a numerical method for solving subsonic flows over a delta wing by assuming atmospheric flight conditions. Near-equilibrium condensation dominated by heterogeneous nucleation is approximated by modifying the condensation model. However, these compressible flow solvers have a certain problem, the so-called stiff problem, when calculating condensate flows at a very low Mach number. No convergence of solution may be obtained. Turkel (1987) along with Choi and Merkle (1993) proposed a preconditioning method to overcome the stiffness in compressible flow solvers.

In this study, the compressible flow solvers (Yamamoto et al., 2000; Yamamoto, 2003) are extended to those for very slow flows by employing the preconditioning method (Turkel, 1987; Choi and Merkle, 1993; Weiss and Smith, 1995; Yamamoto and Shin, 2002) to calculate condensate flows at a very low Mach number. Thus, fundamental equations (except the governing equations for condensation) are transformed to incompressible Navier–Stokes equations and the temperature equation with pseudo-compressibility only at a very low Mach number by using the preconditioning method.

Moreover, a simple experimental apparatus for measuring flows of moist air in a pipe was constructed. The pipe is cooled locally with water vapor in the moist air condensed to water droplets. Condensation in the cooled pipe may be dominated by heterogeneous nucleation where condensed water liquid forms around small particulates in the atmosphere. The number density of the particulates may largely depend on the condensation. Therefore, prediction of the number density may prove quite valuable. However, it may be difficult to directly measure the number densities of particulates and condensed water droplets even by using current experimental methods. From an engineering standpoint, the averaged number density of particulates is alternatively evaluated in this study by using the present numerical method, along with the present experimental apparatus. Then, the difference in relative humidity (i.e., humidity loss) between that at the pipe inlet and that at the pipe outlet was measured under several temperature and humidity conditions by the present experimental apparatus. Flows corresponding to the same conditions were calculated using the present numerical method by changing the number density of particulates at the pipe inlet.

Finally, the proper value of the number density of particulates closest to the value of humidity loss with the experiment is numerically predicted in this study.

2. Numerical methods

2.1. Fundamental equations

Fundamental equations used in this study are based on the two-dimensional compressible Navier–Stokes equations. The set of fundamental equations consists of the conservation laws of total density, the momentums, total energy, density of water vapor, density of water liquid, and number density of the nucleus. Water droplets are assumed to be sufficiently small in this study. Thus, a homogeneous flow without velocity that slips among air, water vapor and water liquid can be assumed. The set of equations are expressed in vector form as

$$\frac{\partial \boldsymbol{q}}{\partial t} + \frac{\partial \boldsymbol{f}_i}{\partial x_i} + \frac{\partial \boldsymbol{f}_{vi}}{\partial x_i} + \boldsymbol{s} = 0 \tag{1}$$

where,

$$\boldsymbol{q} = \begin{bmatrix} \rho \\ \rho u_1 \\ \rho u_2 \\ e \\ \rho_v \\ \rho\beta \\ \rho n \end{bmatrix}, \quad \boldsymbol{f}_i = \begin{bmatrix} \rho u_i \\ \rho u_1 u_i + \delta_{i1} p \\ \rho u_2 u_i + \delta_{i2} p \\ (e+p)u_i \\ \rho_v u_i \\ \rho\beta u_i \\ \rho n u_i \end{bmatrix},$$

$$\boldsymbol{f}_{\mathrm{v}i} = -\begin{bmatrix} 0 \\ \tau_{1i} \\ \tau_{2i} \\ \tau_{ki}u_k + \kappa\partial T/\partial x_i \\ 0 \\ 0 \\ 0 \end{bmatrix}, \quad \boldsymbol{s} = -\begin{bmatrix} 0 \\ 0 \\ 0 \\ 0 \\ -\Gamma_{\mathrm{c}} \\ \Gamma_{\mathrm{c}} \\ \rho I_{\mathrm{c}} \end{bmatrix}$$

$\boldsymbol{q}$, $\boldsymbol{f}_i$, $\boldsymbol{f}_{\mathrm{v}i}$ and $\boldsymbol{s}$ represent the vector of unknown variables, the inviscid flux, viscous flux, and source term, respectively. Eq. (1) is further transformed to equations in terms of general curvilinear coordinates. The set of equations is expressed as

$$Q_t + L(Q) = \frac{\partial Q}{\partial t} + \frac{\partial F_i}{\partial \xi_i} + \frac{\partial F_{\mathrm{v}i}}{\partial \xi_i} + S = 0 \tag{2}$$

where,

$$Q = J\boldsymbol{q}, \quad F_i = J(\partial\xi_i/\partial x_j)\boldsymbol{f}_j, \quad F_{\mathrm{v}i} = J(\partial\xi_i/\partial x_j)\boldsymbol{f}_{\mathrm{v}j},$$
$$S = J\boldsymbol{s}, \quad J = \partial(x_1x_2)/\partial(\xi_1\xi_2)$$

The stress tensor (τ_{ij}) is given by

$$\tau_{ij} = \mu\left[\left(\frac{\partial u_i}{\partial x_j} + \frac{\partial u_j}{\partial x_i}\right) - \frac{2}{3}\delta_{ij}\frac{\partial u_k}{\partial x_k}\right] \tag{3}$$

with flows calculated in this study assumed to be laminar.

The fundamental equations modified by the preconditioning method from Eq. (2) are expressed as general curvilinear coordinates:

$$\Gamma\hat{Q}_t + L(\hat{Q}) = \Gamma\frac{\partial \hat{Q}}{\partial t} + \frac{\partial F_i}{\partial \xi_i} + \frac{\partial F_{\mathrm{v}i}}{\partial \xi_i} + S = 0 \tag{4}$$

where, Γ is the preconditioning matrix. The elements in Γ are fundamentally the same as those of the formulation by Weiss and Smith (1995), and are expressed as

$$\Gamma = \begin{bmatrix} \theta & 0 & 0 & \rho_{\mathrm{T}} & 0 & 0 & 0 \\ \theta u_1 & \rho & 0 & \rho_{\mathrm{T}}u_1 & 0 & 0 & 0 \\ \theta u_2 & 0 & \rho & \rho_{\mathrm{T}}u_2 & 0 & 0 & 0 \\ \theta H - 1 & \rho u_1 & \rho u_2 & \rho_{\mathrm{T}}H + \rho C_p & 0 & 0 & 0 \\ \theta\rho_v/\rho & 0 & 0 & \rho_{\mathrm{T}}\rho_v/\rho & \rho & 0 & 0 \\ \theta\beta & 0 & 0 & \rho_{\mathrm{T}}\beta & 0 & \rho & 0 \\ \theta n & 0 & 0 & \rho_{\mathrm{T}}n & 0 & 0 & \rho \end{bmatrix} \tag{5}$$

where, $H = (e + p)/\rho$. θ is the preconditioning parameter and defined as

$$\theta = 1/U_r^2 - \rho_{\mathrm{T}}/\rho C_p \tag{6}$$

and $\rho_{\mathrm{T}} = \partial\rho/\partial T$. U_r is a switching parameter. If U_r equals the physical speed of sound, θ is zero and the fundamental equations are reduced to the compressible Navier–Stokes equations. $\hat{Q}$ is the vector of unknown primitive variables defined as

$$\hat{Q} = [p \quad u_1 \quad u_2 \quad T \quad \rho_v/\rho \quad \beta \quad n]^{\mathrm{T}}.$$

2.2. Preconditioned flux-difference splitting scheme

Eq. (4) is solved by a finite-difference method based on a preconditioned flux-splitting scheme and a preconditioned LU-SGS scheme (Yamamoto and Shin, 2002). The preconditioned flux-difference splitting method is based on Roe's approximate Riemann solver (Roe, 1981). Then, the numerical flux $(F_i)_{\ell+1/2}$ for F_i in Eq. (4) defined at the interface between control volume ℓ and $\ell+1$ in each coordinate i ($i = 1, 2$), which is derived by a flux-difference splitting form as

$$(\boldsymbol{F}_i)_{\ell+1/2} = \frac{1}{2}\left[\boldsymbol{F}_i\left(\hat{\boldsymbol{Q}}^{\mathrm{L}}_{\ell+1/2}\right) + \boldsymbol{F}_i\left(\hat{\boldsymbol{Q}}^{\mathrm{R}}_{\ell+1/2}\right) - |(\widehat{\boldsymbol{A}}_i)_{\ell+1/2}|\left(\hat{\boldsymbol{Q}}^{\mathrm{R}}_{\ell+1/2} - \hat{\boldsymbol{Q}}^{\mathrm{L}}_{\ell+1/2}\right)\right] \tag{7}$$

where, $\hat{\boldsymbol{Q}}^{\mathrm{L}}$ and $\hat{\boldsymbol{Q}}^{\mathrm{R}}$ are the unknown vectors extrapolated by the compact MUSCL (Yamamoto and Daiguji, 1993) from the left and right directions. The numerical flux of the flux-difference splitting term in Eq. (7) is given by

$$\left|(\widehat{\boldsymbol{A}}_i)_{\ell+1/2}\right|\hat{\boldsymbol{Q}}^{\mathrm{M}} = |\hat{\lambda}_{i1}|\Gamma\hat{\boldsymbol{Q}}^{\mathrm{M}} + \frac{|\hat{\lambda}_{ia}|}{\hat{c}_i\sqrt{g_{ii}}}\hat{\boldsymbol{Q}}_{ia} + \frac{|\hat{\lambda}_{ib}|}{\hat{c}_i^2}\hat{\boldsymbol{Q}}_{ib} \tag{8}$$

Superscript M is replaced by L or R. $g_{ii} = \nabla\xi_i \cdot \nabla\xi_i$. L_i and Λ_i are the matrices composed of preconditioned eigenvectors and preconditioned characteristic speeds (eigenvalues). $|\hat{\lambda}_{ia}|$ and $|\hat{\lambda}_{ib}|$ are defined as

$$|\hat{\lambda}_{ia}| = \left(|\hat{\lambda}_{i3}| - |\hat{\lambda}_{i4}|\right)\Big/2 \tag{9}$$

$$|\hat{\lambda}_{ib}| = \left(\ell_i^-|\hat{\lambda}_{i3}| - \ell_i^+|\hat{\lambda}_{i4}|\right)\Big/(\ell_i^- - \ell_i^+) - |\hat{\lambda}_{i1}| \tag{10}$$

where, $\ell_i^{\pm}$ is calculated by

$$\ell_i^{\pm} = \rho U_r^2/\left(U_i(1-\alpha)/2 \pm \hat{c}_i\sqrt{g_{ii}}\right) \tag{11}$$

$\hat{\lambda}_{ij}$ ($j = 1, 3, 4$) denotes the preconditioned characteristic speeds derived as

$$\hat{\lambda}_{i1} = U_i \tag{12}$$

$$\hat{\lambda}_{i3} = (1+\alpha)U_i/2 + \hat{c}_i\sqrt{g_{ii}} \tag{13}$$

$$\lambda_{i4} = (1+\alpha)U_i/2 - \hat{c}_i\sqrt{g_{ii}} \tag{14}$$

In Eqs. (11), (13) and (14), $\hat{c}_i$ is the numerical speed of sound defined as

$$\hat{c}_i = \sqrt{U_i^2(1-\alpha)^2/g_{ii} + 4U_r^2}/2 \tag{15}$$

and $\alpha = U_r^2(\rho_p + \rho_{\mathrm{T}}/\rho C_p)$, where, $\rho_p = \partial\rho/\partial p$. R is the gas constant. If U_r equals the physical speed of sound, α is reduced to unit, with the characteristic speeds and physical speed of sound for compressible flows being recovered. $\hat{Q}_{ia}$ and $\hat{Q}_{ib}$ are the subvectors defined as

$$\hat{\boldsymbol{Q}}_{ia} = \hat{q}_1^{\mathrm{M}}\boldsymbol{Q}_{ic} + \rho\hat{U}_i\boldsymbol{Q}_d \tag{16}$$

$$\hat{\boldsymbol{Q}}_{ib} = \left(\rho\hat{U}_i\hat{c}_i^2/g_{ii}\right)\boldsymbol{Q}_{ic} + \left(\hat{q}_1^{\mathrm{M}}\hat{c}_i^2/U_r^2\right)\boldsymbol{Q}_d \tag{17}$$

$\hat{q}_j^{\mathrm{M}}$ and $\hat{U}_i$ [$= (\partial\xi_i/\partial x_j)\hat{q}_{j+1}^{\mathrm{M}}$ ($j = 1, 2$)] are the jth element of $\hat{\boldsymbol{Q}}$ and the contravariant velocities are extrapolated by the

compact MUSCL (Yamamoto and Daiguji, 1993) in which M = L or R, respectively. $\boldsymbol{Q}_{ic}$ and $\boldsymbol{Q}_d$ are the subvectors given by

$$\boldsymbol{Q}_{ic} = [\,0 \quad \partial\xi_i/\partial x_1 \quad \partial\xi_i/\partial x_2 \quad U_i \quad 0 \quad 0 \quad 0\,]^{\mathrm{T}} \tag{18}$$

$$\boldsymbol{Q}_d = [\,1 \quad u_1 \quad u_2 \quad H \quad \rho_v/\rho \quad \beta \quad n\,]^{\mathrm{T}} \tag{19}$$

2.3. Preconditioned LU-SGS scheme

The lower–upper symmetric Gauss–Seidel (LU-SGS) scheme (Yoon and Jameson, 1988) is modified to the preconditioned scheme for time integration. The preconditioned LU-SGS can be defined by the following two equations:

$$\Gamma D\Delta\hat{\boldsymbol{Q}}^{*} = \mathrm{RHS} + \Delta t G^{+}(\Delta\hat{\boldsymbol{Q}}^{*}) \tag{20}$$

$$\Delta\hat{\boldsymbol{Q}} = \Delta\hat{\boldsymbol{Q}}^{*} - \Gamma^{-1}\boldsymbol{D}^{-1}\Delta t G^{-}(\Delta\hat{\boldsymbol{Q}}) \tag{21}$$

where, RHS is the vector of explicit time-marching residues of Eq. (4). Δt is the time step. D is the diagonal matrix approximated by the spectral radius of the preconditioned Jacobian matrices. G^{+} and G^{-} are functions composed of time derivatives of numerical flux at neighboring grid points defined as

$$G^{+}(\Delta\hat{Q}^{*}) = \left(\hat{A}_1^{+}\Delta\hat{Q}^{*}\right)_{i-1,j} + \left(\hat{A}_2^{+}\Delta\hat{Q}^{*}\right)_{i,j-1} \tag{22}$$

$$G^{-}(\Delta\hat{Q}) = \left(\hat{A}_1^{-}\Delta\hat{Q}\right)_{i+1,j} + \left(\hat{A}_2^{-}\Delta\hat{Q}\right)_{i,j+1} \tag{23}$$

where, lower scripts i, j indicate a grid point where the time derivative of numerical flux is located. In our approach, these time derivatives on the right side of Eqs. (22) and (23) are calculated by using the preconditioned flux-splitting form developed by Yamamoto and Shin (2002).

2.4. Condensation model

The equation of state used in this study has been derived by Ishizaka et al. (1994), by assuming that the mass fraction of water liquid β is sufficiently small ($\beta < 0.1$). This equation is given by

$$p = \rho RT(1-\beta) \tag{24}$$

Moist air occasionally condenses in wind tunnel experiments. The onset of condensation may be dominated by homogeneous nucleation. Homogeneous nucleation occurs suddenly from pure water vapor without a nucleus in a high-supersaturated condition. Conversely, heterogeneous nucleation and almost equilibrium condensation may govern the natural condensation observed in atmospheric weather conditions. Yamamoto (2003) developed a simple condensation model for simulating condensate flows of moist air under atmospheric flight conditions. In this study, this model is applied to the present flow problems. Thus, the mass generation rate (Γ_c) of water droplets in Eq. (1) is formed as the growth rate of a water droplet approximated by Ishizaka et al. (1994) as

$$\Gamma_c = 4\pi\rho_\ell n r^2 \frac{\mathrm{d}r}{\mathrm{d}t} \tag{25}$$

where, ρ_ℓ is the density of water liquid. The growth rate of a water droplet ($\mathrm{d}r/\mathrm{d}t$) is given by the Hertz–Knudsen model in which the droplet radius is much smaller than the mean free path of a vapor molecule. The approximate model proposed by Schnerr and Dohrmann (1990) is employed here. The saturation pressure for a water droplet of radius r is given by the Kelvin–Helmholtz equation. In this study for simplifying the present flow problem, we assume that a constant number of particulates with a constant radius are uniformly included in atmospheric flow conditions. Therefore, the value of the number density of particulates n in Eq. (1) is actually set to a constant value in the whole flow field in this study.

3. Experimental apparatus

Fig. 1 shows the experimental apparatus used in this study. The working air provided from a chemical plant includes a finite amount of small particulates. One ultimate purpose of this study is to predict corrosion in the chemical plant induced by the condensation of water vapor containing reacting chemicals. In this case, however, no reacting chemicals are included in the wet air. The apparatus consists of three sections: the moist generation section (to control the humidity and temperature of wet air), the test section (to control surface temperature of the pipe locally covered with a cooling jacket and immersed in a water bath with a pre-heater), and the detection section (to control the temperature of outlet air to recover the same temperature as that of the inlet air). The relative humidity of the plant air is regulated to less than 3%. The dry air passes through the vapor phase of the water vessel. Relative humidity then increases to 50%. The temperature controller regulates the temperature of water in the water vessel. The aluminum pipe measures 800 mm in length, with an outer diameter of 37 mm and a bore of 35 mm. A 400-mm channel in the pipe (from the pipe inlet to the end of the heating part) is prefaced to sufficiently form the flow boundary layer. The temperature of the heating part on the pipe wall is maintained at ambient temperature by the water bath. The cooling part on the pipe wall is covered with the cooling jacket to adjust wall temperature from −5 to −15 °C. A solution of ethyleneglycol or methanol and distilled water is used as the refrigerant. The outlet flow (after passing through the cooled pipe) is heated again by streaming in the helical copper tube attached after the cooled pipe. This tube is heated to ambient temperature because humidity loss in the pipe must be evaluated at the same temperature as that of the inlet flow. Type-T thermocouples and humidity sensors measure the temperature and relative humidity, respectively. Moreover, Type-T thermocouples measure the radial distributions of temperature at three points at the cooled pipe outlet. Then, the helical copper tube is detached from the cooled pipe. Experiments are conducted

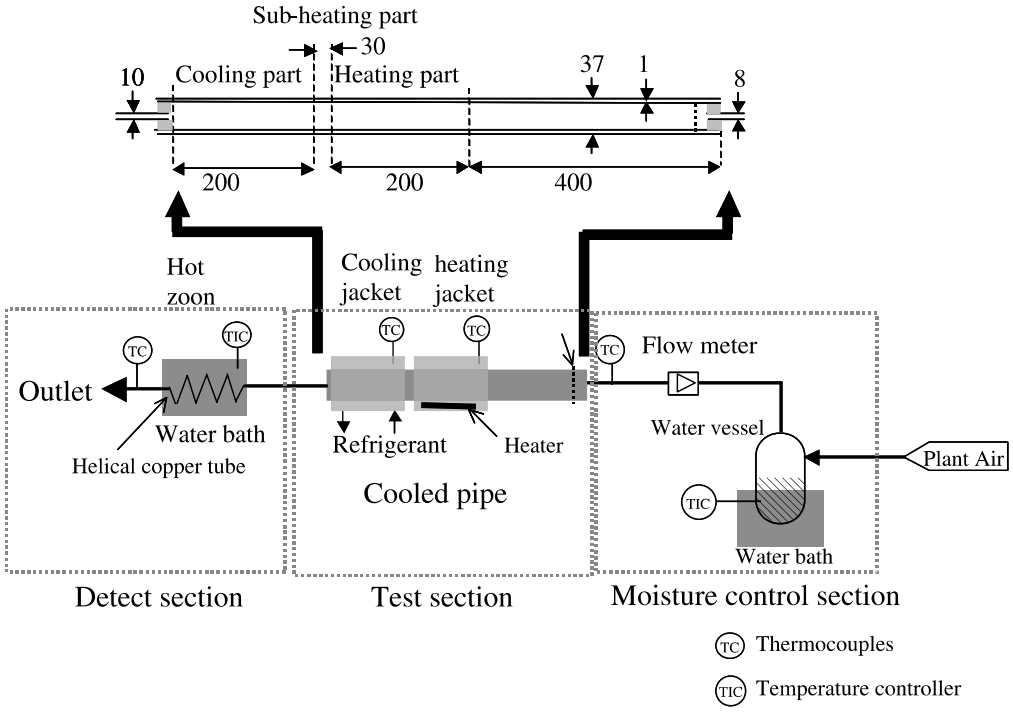

Fig. 1. Schematic of the experimental apparatus.

to measure the outlet temperature of the cooled pipe and relative humidity by varying the temperature of the cooling part of the pipe wall. The relative humidity at the inlet is far less than 100% (saturated). The flow is very slow, with a small difference between the cooling temperature and ambient temperature. Therefore, homogeneous nucleation never occurs in the present experiments.

4. Calculated results

Very slow flows of moist air in the cooled pipe used in the experiments above are calculated using the present method. The flow is simplified as flowing only through an axisymmetric pipe in which the outer wall is partially cooled. The axisymmetric term is added in Eq. (1). Fig. 2 shows the schematic of the cooled pipe and the computational grid. The pipe is 400 mm in length and 35 mm in diameter. The right half of the pipe wall is cooled; the left half is maintained at the same temperature as that at the pipe inlet. The computational grid forms a rectangular H-type grid. Two-dimensional 201×41 grid points are generated, assuming an axisymmetric flow. Grid points are concentrated on the wall to resolve the boundary layer. The actual inlet flow in the experiment enters the pipe after streaming through a narrow tube as shown in Fig. 1. In the calculation, however, the prefaced narrow tube is not considered sufficient to simplify the problem. The problem of condensation occurring here is supposed to be governed by heterogeneous nucleation. The simplified model developed by Yamamoto (2003) is used. The effect of surface tension (on the inner wall of the pipe) on condensation is not considered. Table 1 lists the flow conditions considered in this study. The cooled wall temperature and number density of particulates in moist air through the pipe are also changed. The inlet temperature is fixed at 288.15 K and the inlet relative humidity is 50% as conducted by the experiment. To determine the inlet flow speed, the value of temperature at the axis of the pipe outlet (measured by the experiment) is referred to in the calculation. Then, the inlet flow speed that can recreate the value of temperature closest to that

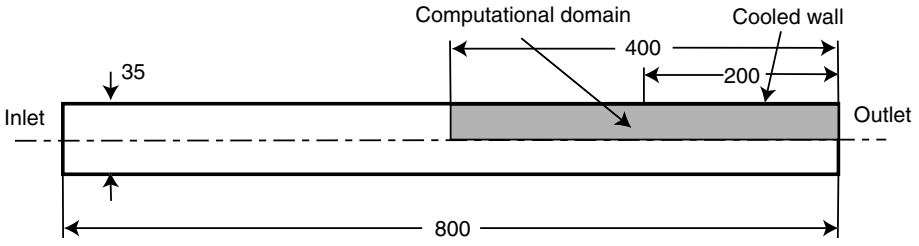

Fig. 2. Schematic of the cooled pipe and the computational grid.

Table 1
Flow conditions

CASE	Cold wall temperature (K)	Number density of particulates ($1/m^3$)
A1	268.15	1E10
A2		1E11
A3		1E12
B1	263.15	1E10
B2		1E11
B3		1E12
C1	258.15	1E10
C2		1E11
C3		1E12

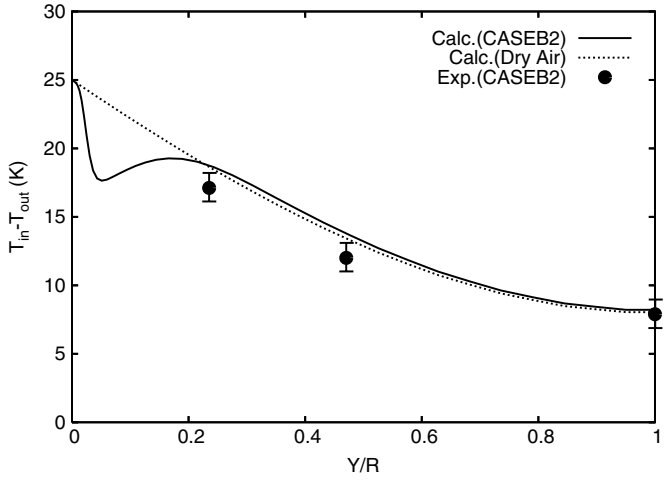

Fig. 3. Calculated temperature differences $T_{in} - T_{out}$ at the outlet of the pipe compared with the experiments.

obtained by the experiment was chosen through certain pre-calculations based on CASEB2 in Table 1. Consequently, a Reynolds number of 102 was determined.

The calculated results of CASEB2 are first compared with the corresponding experimental results and calculated results, assuming no condensation (dry air). Fig. 3 shows the calculated temperature functions at the pipe outlet defined by $T_{in} - T_{out}$, where T_{in} is the inlet temperature and T_{out} the outlet temperature. Y/R is the nondimensional distance from the pipe wall to the axis of the pipe. The calculated values at the axis of the pipe are in good agreement with the experiment due to specifying the previously expressed inlet flow speed. Calculated values at other two points are somewhat overestimated from the values measured by the experiment. However, it should be noted here that the experimental data included errors when the measurement was conducted. Specifically, each value of T_{in} and T_{out} in the experiment has a ± 0.5 °C margin of error in temperature. Therefore, ± 1 °C in the function $T_{in} - T_{out}$ may be estimated as the maximum error. Moreover, the relative humidity measured with the humidity sensor (i.e., RH value in the experiment) has $\pm 1.6\%$ error. This includes the essential measuring error ($\pm 1\%$) of the analyzer, and error ($\pm 0.6\%$) caused by the error in temperature. The

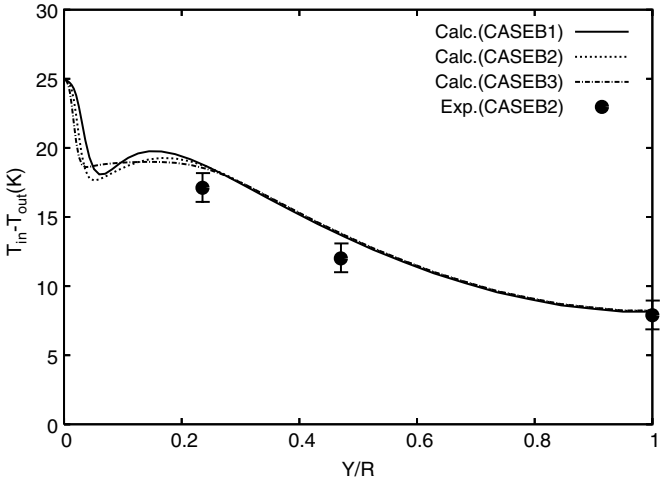

Fig. 4. Calculated temperature differences $T_{in} - T_{out}$ at the outlet of the pipe in CASEB1, B2, and B3 compared with the experiments.

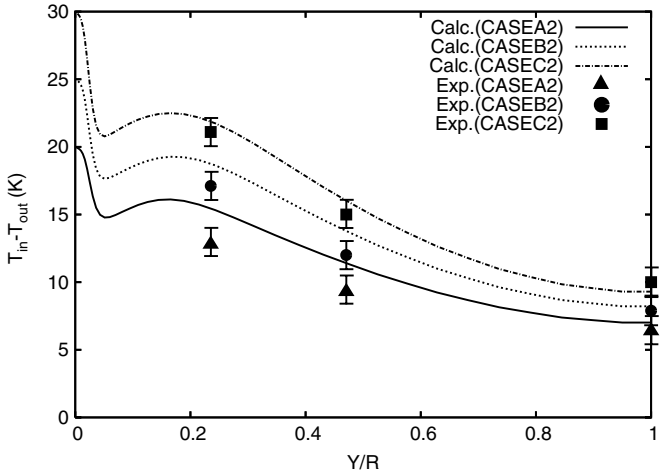

Fig. 5. Calculated temperature differences $T_{in} - T_{out}$ at the outlet of the pipe in CASEA2, B2, and C2 compared with the experiments.

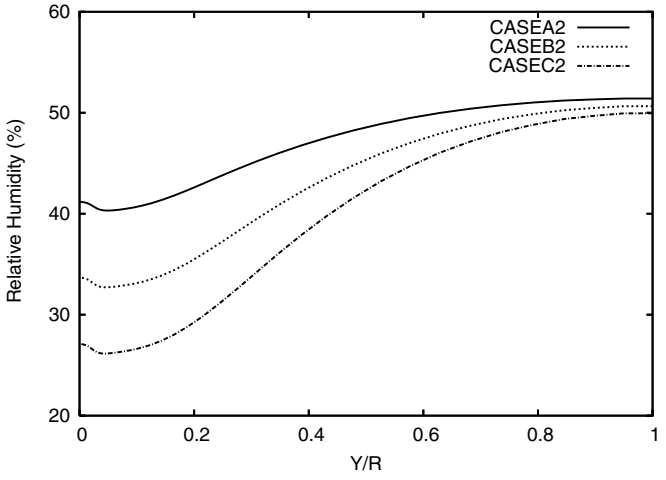

Fig. 6. Calculated relative humidity distributions at the outlet of the pipe in CASEA2, B2, and C2.

calculated value of CASEB2 is almost the same as that obtained by assuming dry air at $0.2 < Y/R$. However, the difference at $Y/R < 0.2$ is large because the difference is associated with the release of latent heat due to condensation in this flow region. The released heat increases the temperature in the surrounding region, which results in a decrease in the value defined by $T_{in} - T_{out}$.

Next, the effect of small particulates in moist air on temperature distribution at the pipe outlet is investigated. Fig. 4 shows the calculated values of $T_{in} - T_{out}$ corresponding to the previous case in CASEB1, B2, and B3, respectively. The increase in the number density of small particulates slightly influences temperature distribution only at $Y/R < 0.2$. Fig. 5 also compares the calculated values in CASEA2, B2, and C2 with the corresponding experiments. As temperature at the cooled wall decreases,

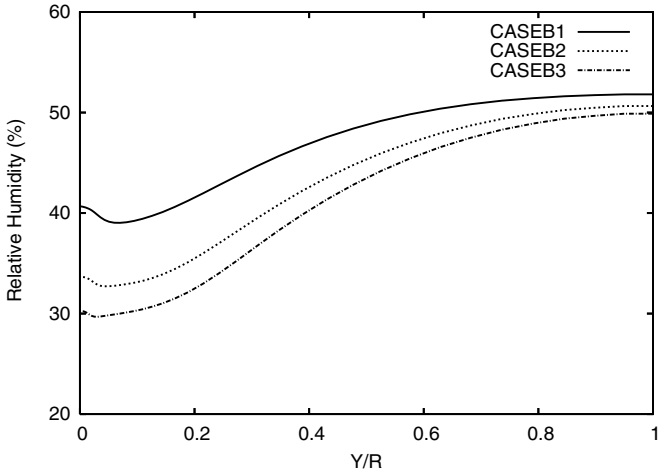

Fig. 7. Calculated relative humidity distributions at the outlet of the pipe in CASEB1, B2, and B3.

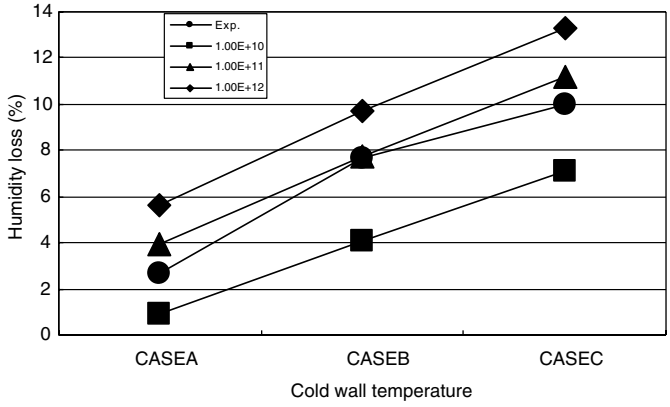

Fig. 8. Calculated humidity loss at the outlet of the pipe compared with the experiments.

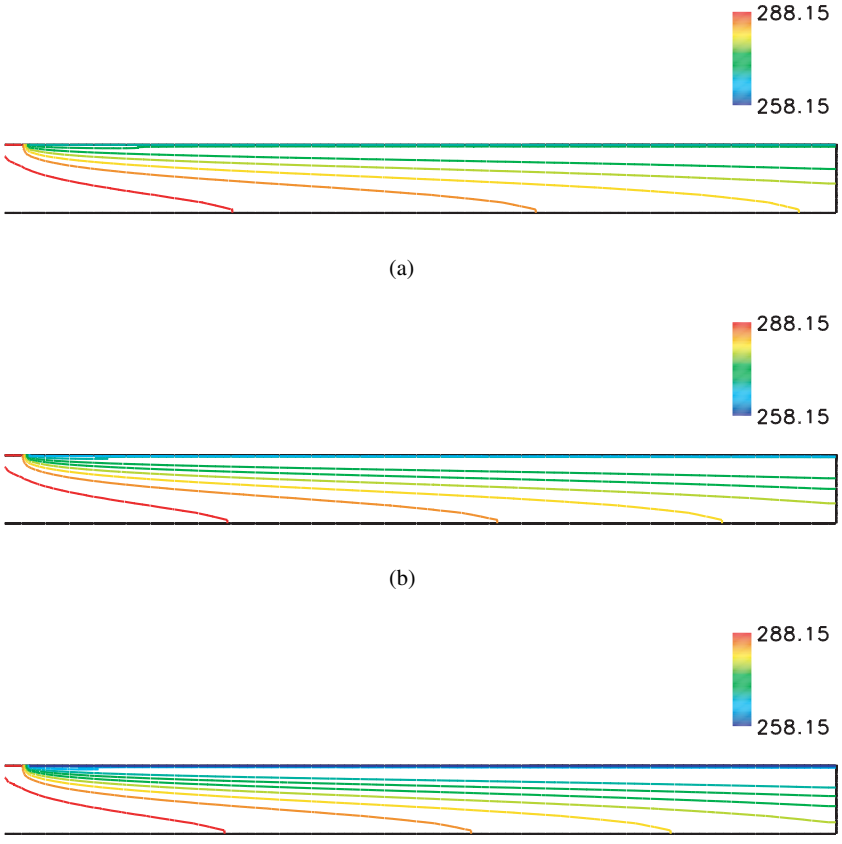

Fig. 9. Calculated temperature contours at right half and upper region in the pipe: (a) CASEA2, (b) CASEB2 and (c) CASEC2.

the value of $T_{in} - T_{out}$ increases. A similar increase in $T_{in} - T_{out}$ was also found in the experiments.

The calculated relative humidity is also shown here to clarify the effects of cooling by the cooled wall and the small particulates in moist air on condensation. Fig. 6 shows the calculated relative humidity in CASEA2, B2, and C2 at the pipe outlet. The relative humidity is defined as p_v/p_s, where p_v is the vapor pressure and p_s the saturation pressure of water vapor as evaluated by inlet temperature. The value of relative humidity gradually decreases toward the wall because a finite amount of water vapor in moist air changes to water liquid due to condensation, and then the vapor pressure decreases. The decrease in temperature at the cooled wall also increases water liquid and decreases relative humidity. Fig. 7 shows the calculated relative humidity in CASEB1, B2, and B3 at the pipe outlet. As the number density of particulates increases, the relative humidity at the pipe outlet tends to decrease. The calculated results in this study thus indicate that the number density of particulates has a significant effect on condensation.

Fig. 8 compares the calculated humidity loss (defined as $\phi_{in} - \phi_{out}$, where ϕ_{in} is relative humidity at the pipe inlet and ϕ_{out} the average relative humidity at the pipe outlet) with the corresponding experiments. For both values, the saturation pressure of water vapor is evaluated by inlet temperature. The calculated values for all nine cases in Table 1 are plotted in Fig. 8. As temperature decreases at the cooled wall, the calculated humidity loss increases in all three cases, thus changing the number density of particulates. A similar tendency was also found in the experiments. As the number density of particulates increases, the calculated humidity loss also increases. The values obtained by the experiments may approximate the calculated values, by assuming 1E11 m^{-3} as the number density of particulates. Consequently, the present method of setting the number density of particulates to 1E11 m^{-3} could accurately recreate the findings of the present experiments.

The calculated temperature contours in CASEA2, B2, and C2 are shown in (a)–(c), respectively, in Fig. 9. Only those in the right half and upper region of the pipe shown in Fig. 2 are visualized. Flows are gradually cooled through the cooled region of the pipe. The lower temperature at the cooled wall cools the moist air more than at the pipe outlet. The calculated condensate mass fraction contours corresponding to (a)–(c) in Fig. 9 are also shown in (a), (b), and (c) in Fig. 10. Thus, it was determined that the region where condensation occurs is limited to that near the cooled wall. The condensate boundary layer grows and the mass of water liquid gradually increases along the cooled wall. The condensate mass also increases as temperature decreases at the cooled wall of the pipe.

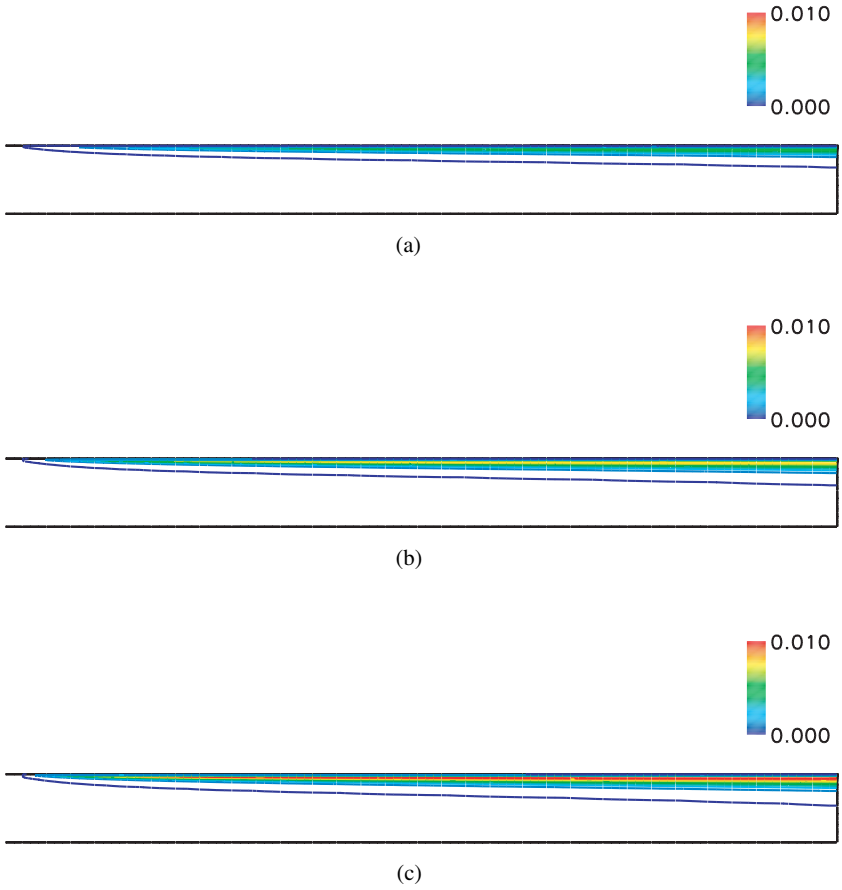

Fig. 10. Calculated condensate mass fraction contours at right half and upper region in the pipe: (a) CASEA2, (b) CASEB2 and (c) CASEC2.

5. Concluding remarks

Numerical and experimental studies on condensation in a cooled pipe when streams of moist air flow through the pipe were presented. The numerical method developed is based on the preconditioning method, fundamental equations, and models for condensate flows. The present calculations (assuming heterogeneous condensation where small particulates are included in the atmosphere) could well recreate condensation in the present problem as conducted by the experiments. Consequently, it was determined that the number density of particulates set in the present method is largely dependent on condensation, and that 1E11 m^{-3} was the most proper value to recreate the present flow problems.

References

Choi, Y.-H., Merkle, C.L., 1993. The application of preconditioning in viscous flows. Journal of Computational Physics 105, 207–223.

Hill, P.G., 1966. Condensation of water vapor during supersonic expansion in nozzles. Journal of Fluid Mechanics 25, 593–620.

Ishizaka, K., Ikohagi, T., Daiguji, H., 1994. A high-resolution finite difference scheme for supersonic wet-stream flows. Transaction of JSME, Series B 60, 3887–3892 (in Japanese).

Moses, C.A., Stein, G.D., 1978. On the growth of steam droplets formed in a laval nozzle using both static pressure and light scattering measurements. Transaction of ASME, Journal of Fluids Engineering 100, 311–322.

Roe, P.L., 1981. Approximate Riemann solvers, parameter vectors, and difference schemes. Journal of Computational Physics 43, 357–372.

Schnerr, G.H., 1989. 2-D transonic flow with energy supply by homogeneous condensation: onset condition and 2-D structure of steady laval nozzle flow. Experiments in Fluids 7, 145–156.

Schnerr, G.H., Dohrmann, U., 1990. Transonic flow around airfoils with relaxation and energy supply by homogeneous condensation. AIAA Journal 28, 1187–1193.

Turkel, E., 1987. Preconditioned methods for solving the incompressible and low speed compressible equations. Journal of Computational Physics 72, 277–298.

Weiss, J.M., Smith, W.A., 1995. Preconditioning applied to variable and constant density flows. AIAA Journal 33, 2050–2057.

Yamamoto, S., 2003. Onset of condensation in vortical flow over sharp-edged delta wing. AIAA Journal 41, 1832–1835.

Yamamoto, S., Daiguji, H., 1993. Higher-order-accurate upwind schemes for solving the compressible Euler and Navier–Stokes equations. Computers & Fluids 22, 259–270.

Yamamoto, S., Shin, B.-R., 2002. Preconditioned implicit flux-splitting scheme for condensate flows. In: Proceedings of 2nd International Conference on Computational Fluid Dynamics—Sydney, Springer, pp. 112–117.

Yamamoto, S., Hagari, H., Murayama, M., 2000. Numerical simulation of condensation around the 3-D wing. Transaction of Japan Society for Aeronautical and Space Sciences 42, 182–189.

Yoon, S., Jameson, A., 1988. Lower–upper symmetric-Gauss–Seidel method for the Euler and Navier–Stokes equations. AIAA Journal 26, 1025–1026.

Young, J.B., 1992. Two-dimensional, nonequilibrium, wet-steam calculations for nozzles and turbine cascades. Transaction of ASME, Journal of Turbomachinery 114, 569–579.